C. R. Mecanique 343 (2015) 656–669

Contents lists available at ScienceDirect

Comptes Rendus Mecanique

www.sciencedirect.com

Acoustic metamaterials and phononic crystals

Nonlocal description of sound propagation through an array of Helmholtz resonators

Description non locale de la propagation du son dans une chaîne de résonateurs de Helmholtz

Navid Nemati [a,*], Anshuman Kumar [a], Denis Lafarge [b], Nicholas X. Fang [a]

[a] *Department of Mechanical Engineering, Massachusetts Institute of Technology, 77 Massachusetts Avenue, Cambridge, MA 02139, USA*
[b] *Laboratoire d'acoustique de l'université du Maine, UMR 6613, avenue Olivier-Messiaen, 72085 Le Mans cedex 9, France*

ARTICLE INFO

Article history:
Received 22 January 2015
Accepted 22 May 2015
Available online 18 June 2015

Keywords:
Helmholtz resonators
Acoustic metamaterials
Nonlocal description
Spatial dispersion
Viscothermal fluid
Negative modulus

Mots-clés :
Résonateur d'Helmholtz
Métamatériaux acoustiques
Description non locale
Dispersion spatiale
Fluide viscothermique
Module de compressibilité négatif

ABSTRACT

A generalized macroscopic nonlocal theory of sound propagation in rigid-framed porous media saturated with a viscothermal fluid has been recently proposed, which takes into account both temporal and spatial dispersion. Here, we consider applying this theory, which enables the description of resonance effects, to the case of sound propagation through an array of Helmholtz resonators whose unusual metamaterial properties, such as negative bulk moduli, have been experimentally demonstrated. Three different calculations are performed, validating the results of the nonlocal theory, related to the frequency-dependent Bloch wavenumber and bulk modulus of the first normal mode, for 1D propagation in 2D or 3D periodic structures.

RÉSUMÉ

Une théorie macroscopique nonlocale générale de la propagation du son dans les milieux poreux à structure rigide saturés par un fluide viscothermique a récemment vu le jour. Tenant un compte complet des dispersions, tant temporelles que spatiales, elle décrit entièrement les résonances. Nous l'appliquons ici au cas de la propagation du son dans un réseau de résonateurs de Helmholtz, dont les propriétés non usuelles (modules de compressibilité négatifs) ont été établies expérimentalement. Trois calculs différents sont présentés, qui valident les résultats de la théorie non locale, relatifs au nombre d'onde et module de compressibilité, qui sont fonctions de la fréquence, du mode de Bloch principal (le moins atténué), pour une propagation 1D en géométries périodiques 2D ou 3D.

* Corresponding author.
E-mail addresses: nnemati@mit.edu (N. Nemati), akumr@mit.edu (A. Kumar), denis.lafarge@univ-lemans.fr (D. Lafarge), nicfang@mit.edu (N.X. Fang).

http://dx.doi.org/10.1016/j.crme.2015.05.001
1631-0721/

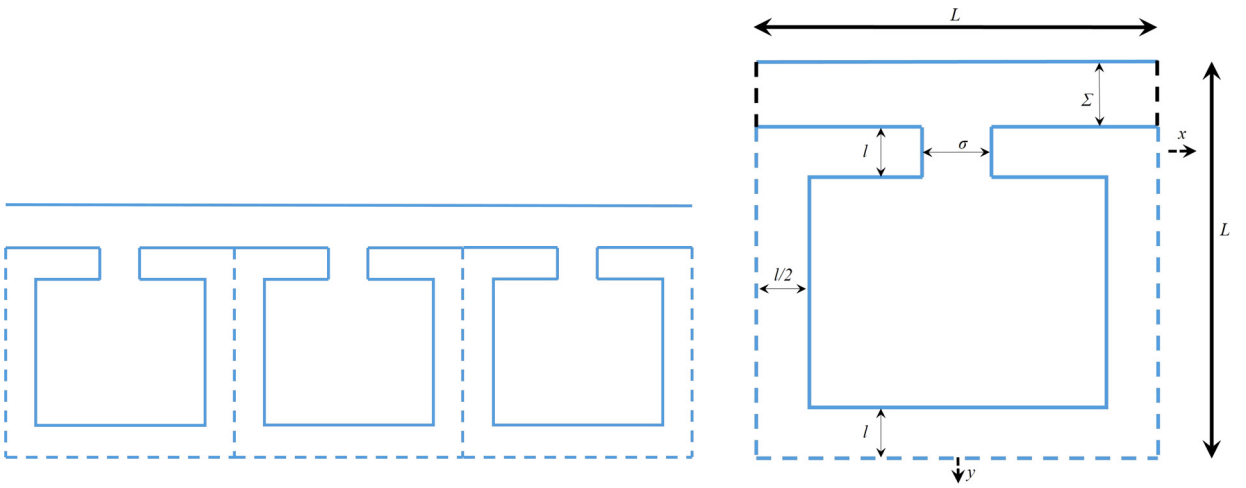

Fig. 1. (Color online.) Left: illustration of a 2D array of Helmholtz resonators. Right: a periodic cell of the structure, with $L = 1$ cm, $\Sigma = 0.2L$, $\sigma = 0.015L$, and $l = 0.15L$.

1. Introduction

We employ here a generalized macroscopic nonlocal theory of sound propagation in rigid-framed porous media saturated with a viscothermal fluid [1] to describe the behavior of an acoustic metamaterial made of an array of Helmholtz resonators filled with air (see Fig. 1 left). Inspired by the electromagnetic theory and a thermodynamic consideration relating to the concept of acoustic part of energy current density, this macroscopic theory allows us to go beyond the limits of the classical local theory and within the limits of linear theory, to take into account not only temporal dispersion, but also spatial dispersion. By *macroscopic theory* we mean that the theory is concerned with averaged fields only. Assuming that there is a suitable ensemble of realizations of the medium, the macroscopic theory then is developed to describe the dynamics of the ensemble-averaged fields. A special case will be that of a periodic medium. The ensemble will be the collection of configurations generated by random translations of a single sample, and the ensemble average will be related to cell average of one sample. In the framework of the new approach, a homogenization procedure is proposed, through solving two independent microscopic action-response problems each of which related to the effective density and effective bulk modulus of the material. Contrary to the classical (two-scale asymptotic) method of homogenization, no asymptotic approach has been employed and there is no length-constraint to be considered within the development of the new method. Thus, there would be no frequency limit for the medium effective properties to be valid; in addition, materials with different length scales can be treated. The homogenization procedure offers a systematic way of obtaining the effective properties of the materials, regardless of their geometries. These characteristics of the nonlocal approach permits the description of the porous media with specific geometries causing metamaterial behavior. A metamaterial with periodic structure will be studied: two-dimensional and three dimensional chain of Helmholtz resonators connected in series.

By local theory, we refer to space locality. Nonlocality in time, or temporal dispersion, has been already taken into account through models for wave propagation in porous media [2–5]. That is, in Fourier space the effective density and bulk modulus depend on the frequency ω. In other words, the field dynamics at one location retains a memory of the field values at this location but is not affected by the neighboring values. The local description is usually based on retaining only the leading order terms in the two-scale homogenization method [6–11,5]. An asymptotic two-scale approach is applied in terms of a characteristic length of the medium, the period L in periodic media, which is assumed to be much smaller than the wavelength λ [12,13]. Efforts have been performed to extend the asymptotic method of homogenization to higher frequencies for the periodic composite materials [14,15] and rigid porous media [16] by introducing another type of scale separation to which the asymptotic multi-scale procedure applies. An enhanced asymptotic method has been adapted to describe sound propagation in rigid porous media with embedded damped Helmholtz resonators [17] exhibiting scattering different from Bragg scattering at high frequency in periodic media.

An effective medium approach has been proposed for periodic elastic composites based on surface responses of a structural unit of the material [18], which can describe the macroscopic parameters beyond the frequencies within the long wavelength limit. Unlike the classical methods, based on the introduction of two-scale asymptotic expansions, or coherent potential approximation [19] based on the effective-medium parameters minimizing scatterings in the long-wavelength limit, the homogenization scheme presented in [18] uses matching the lowest-order scattering amplitudes arising from a periodic unit cell of the metamaterial with that of a homogenized material. As such, local resonant scattering can be captured as well by the latter method in the elastic metamaterials. The asymptotic method of homogenization has been enhanced to provide the weak nonlocal effects as a small correction to the local behavior [20]. An approach has been presented [21] for random elastic composites based on ensemble averaging of the material responses to a body force, giving rise to effective

parameters of the medium depending on frequency and wavenumber. By this method, the case of periodic media can be treated as well.

The nonlocal theory we use here takes fully the temporal dispersion and spatial dispersion into account. The medium is assumed unbounded and homogeneous in the stationary random statistical sense; therefore, the spatial dispersion refers only to the dependence of the permittivities, i.e. effective density and bulk modulus, on the Fourier wavenumbers $\boldsymbol{k}$ present in the macroscopic fields [22]. As mentioned above, the theory can be applied with certain considerations to a periodic medium; in particular it gives the Bloch wavenumbers and defines Bloch impedances. The materials susceptible to showing the nonlocal behavior may be classified into two main groups regarding their microgeometry. The first comprises the materials which exhibit this behavior in sufficiently high frequency regime. The second one concerns materials with microgeometry constituting the resonators, which exhibit spatial dispersion phenomena even at not very high frequencies; the resonance phenomena act as a source generating nonlocal behavior. In this article, we investigate the second type of these geometries in the form of daisy-chained Helmholtz resonators. We will see the first one in a forthcoming paper, where 1D propagation in a two-dimensional lattice of rigid cylinders will be studied. A material made of an array of Helmholtz resonators filled by water has been studied experimentally, and has been found to show negative bulk modulus in the resonance frequency range [23]. Later, Helmhotz resonators as structural units were used to design novel metamaterials for focusing ultrasound waves [24] and broadband acoustic cloaking [25].

Here, we apply the nonlocal theory to quantitatively describe the macroscopic dynamics of such a metamaterial filled with air as a viscothermal fluid, in 2D as well as in 3D. For the 2D case, using a simplified analytical solution of the complete equations, we present the method of obtaining the nonlocal effective density and effective bulk modulus. When these effective parameters satisfy the dispersion equation based on the nonlocal theory, we can compute the wavenumber of the least attenuated mode, among other modes. We can then check that the wavenumber resulting from the macroscopic nonlocal theory coincides with the wavenumber associated with the Bloch wave propagating and attenuating in the medium. The Bloch solution is determined using the same simplifying way of solving as in the nonlocal modeling. Thus the results based on the two calculations should be comparable. Finally, as a check of the validity of the simplifying assumptions introduced in our modeling calculations, we have performed direct Finite Element Method (FEM) computations based on the exact equations in the framework of nonlocal homogenization.

In Section 2, we review briefly the general framework of the nonlocal theory which is used in this paper. The microscopic equations governing sound propagation in a rigid porous medium are summarized, before mentioning the macroscopic Maxwellian equations describing the macroscopic nonlocal dynamics of the homogenized equivalent fluid. In Section 3, we will see the nonlocal modeling allowing the calculation of the effective parameters and the wavenumber of the least attenuated wave in the medium. The direct calculation of the Bloch wavenumber, using similar simplifications, is presented in Section 4. Section 5 is devoted to the results of the three different calculations in 2D, and also the results based on the nonlocal modeling and Bloch wave calculations which have been generalized to 3D structures.

2. General framework of the nonlocal theory

In the following, we state the microscopic equations applied at the pore level, and the nonlocal Maxwellian macroscopic equations that describe the dynamics of the material as a homogeneous equivalent fluid medium. Then, we recall briefly the upscaling procedures allowing to obtain the frequency and wavenumber dependent effective parameters of the macroscopic equivalent fluid medium, i.e. effective density and effective bulk modulus. This section is a summary of the results which have been discussed in detail in [1]. Hence, we will frequently refer to [1], for the in-depth explanations.

2.1. Microscopic equations

The dynamics of a small amplitude perturbation in a rigid-framed porous material filled with a viscothermal fluid is governed by the linearized equations of the mass, momentum, and energy balance, and a general fluid state equation as follows: in the fluid region $\mathcal{V}^f$

$$\rho_0 \frac{\partial \boldsymbol{v}}{\partial t} = -\nabla p + \eta \nabla^2 \boldsymbol{v} + (\zeta + \frac{\eta}{3}) \nabla (\nabla \cdot \boldsymbol{v}) \tag{1a}$$

$$\frac{\partial b}{\partial t} + \nabla \cdot \boldsymbol{v} = 0 \tag{1b}$$

$$\gamma \chi_0 p = b + \beta_0 \tau \tag{1c}$$

$$\rho_0 c_p \frac{\partial \tau}{\partial t} = \beta_0 T_0 \frac{\partial p}{\partial t} + \kappa \nabla^2 \tau \tag{1d}$$

where $\boldsymbol{v}$, $b \equiv \rho/\rho_0$, p and τ, are the fluid velocity, excess condensation, thermodynamic excess pressure, excess temperature, respectively, and ρ is the excess density. The fluid constants ρ_0, η, ζ, γ, χ_0, β_0, c_p, T_0, κ, represent the ambient density, first viscosity, second viscosity, ratio of the heat capacity at constant pressure to heat capacity at constant volume c_p/c_v, adiabatic compressibility, coefficient of thermal expansion, specific heat capacity per unit mass at constant pressure, ambient temperature, and coefficient of thermal conduction, respectively.

In the (rigid) solid phase region $\mathcal{V}^s$, energy balance equation is reduced to $\rho^s c_p^s(\partial\tau^s/\partial t) = \kappa^s\nabla^2\tau^s$, where ρ^s is the constant solid density, τ^s solid excess temperature, and κ^s solid coefficient of thermal conductivity. On the fluid/solid interface $\partial\mathcal{V}$, we have the conditions of continuity of the excess temperature $\tau = \tau^s$ and the heat flux $\kappa\nabla\tau = \kappa^s\nabla\tau^s$. We admit that the coefficient of thermal conductivity of the solid is much larger than that of the fluid $\kappa^s \gg \kappa$, and the heat capacity at constant pressure of the solid part is much larger than that of the fluid part, i.e., $(1-\phi)\rho^s c_p^s \gg \phi\rho_0 c_p$; where ϕ is the fluid volume fraction (porosity). The latter assumptions combined with the Fourier heat diffusion in the solid, and the temperature and heat flux continuity relations, generally result in the vanishing of the fluid excess temperature at the fluid/solid boundaries. In addition, we assume no-slip condition on the fluid/(rigid) solid interface. The boundary conditions for the velocity and excess temperature on $\partial\mathcal{V}$ are finally written as

$$\boldsymbol{v} = 0, \quad \tau = 0 \tag{2}$$

2.2. Macroscopic Maxwellian acoustics

Before going through the macroscopic equations for sound propagation in rigid-framed porous media, and the homogenization procedure, we will precise the notion of field averaging in the nonlocal approach.

Averaging: The present macroscopic theory is statistical in nature and has been developed in principle for fluid-saturated rigid-framed media which are homogeneous in an ensemble-averaged sense; this is the case of stationary random media. The macroscopic properties represented in the theory refer to the ensemble of realizations. Thus, for example, the propagation constants of the medium would refer to the propagation constant of *coherent waves* in multiple-scattering theory. Here, the material we wish to study is not defined by stationary random realizations. It belongs to the important class of periodic materials. The macroscopic theory can still be applied by considering the ensemble obtained through random translation of one sample. It turns out that the ensemble-average $\langle\,\rangle$ properties of the space are, in this case, precisely computable by spatial averaging over a periodic cell in a single realization. This, in a sense, reminds of *ergodicity* in stationary random media.

The macroscopic condensation and velocity are defined as the average of pore scale microscopic fields: $\boldsymbol{V} \equiv \langle\boldsymbol{v}\rangle$, and $B \equiv \langle b\rangle$; average over the periodic cell in the case of the periodic media. A macroscopic equation can be obtained directly by averaging Eq. (1b), using the commutation relation $\langle\boldsymbol{\nabla}.\boldsymbol{v}\rangle = \boldsymbol{\nabla}.\langle\boldsymbol{v}\rangle$ which is automatically satisfied owing to (2) (see Eq. (56) in [1]). The second macroscopic field equation, as well as the macroscopic constitutive relations, are written using the electromagnetic analogy. This analogy suggests that the system of macroscopic equations can be carried through by introducing new Maxwellian fields H and $\boldsymbol{D}$, as well as linear operators $\hat{\rho}$ and $\hat{\chi}^{-1}$. The field equations and constitutive relations are written as (see section 3.3 in [1])

$$\textbf{Field equations:} \qquad \frac{\partial B}{\partial t} + \nabla\cdot\boldsymbol{V} = 0, \qquad \frac{\partial \boldsymbol{D}}{\partial t} = -\nabla H \tag{3}$$

$$\textbf{Constitutive relations:} \quad \boldsymbol{D} = \hat{\rho}\boldsymbol{V}, \qquad H = \hat{\chi}^{-1}B \tag{4}$$

where the integral operators of density $\hat{\rho}$ and bulk modulus $\hat{\chi}^{-1}$ are such that

$$\boldsymbol{D}(t,\boldsymbol{r}) = \int_{-\infty}^{t} \mathrm{d}t' \int \mathrm{d}\boldsymbol{r}'\rho(t-t',\boldsymbol{r}-\boldsymbol{r}')\boldsymbol{V}(t',\boldsymbol{r}') \tag{5a}$$

$$H(t,\boldsymbol{r}) = \int_{-\infty}^{t} \mathrm{d}t' \int \mathrm{d}\boldsymbol{r}'\chi^{-1}(t-t',\boldsymbol{r}-\boldsymbol{r}')B(t',\boldsymbol{r}') \tag{5b}$$

We notice that the kernels ρ and χ^{-1} depend on the difference $t-t'$ and $\boldsymbol{r}-\boldsymbol{r}'$, which is due to the homogeneity in time and material space. Therefore, we can write (5a) and (5b) in the Fourier space, respectively, as

$$\boldsymbol{D}(\omega,\boldsymbol{k}) = \rho(\omega,\boldsymbol{k})\boldsymbol{V}(\omega,\boldsymbol{k}), \qquad H(\omega,\boldsymbol{k}) = \chi^{-1}(\omega,\boldsymbol{k})B(\omega,\boldsymbol{k}) \tag{6}$$

In nonlocal theory, the macroscopic H field is defined through the Poynting–Schoch condition of *acoustic part of energy current density* [1,26] which is postulated as (see section 3.4 in [1]):

$$S = H\boldsymbol{V} = \langle p\boldsymbol{v}\rangle \tag{7}$$

As a result of this definition, the operators density and bulk modulus become susceptibility functions determinable in principle through independent action-response problems (see Section 2.4 in [1]). Regarding Eqs. (5) and (6), it is visible that the theory allows for both temporal dispersion, shown by integration over time variable t' in physical space and frequency dependence in Fourier space, and spatial dispersion, shown by integration over space coordinates $\boldsymbol{r}'$ and wavenumber dependence in Fourier space. We will recognize the quantities in physical space $(t,\boldsymbol{r})$ and Fourier space $(\omega,\boldsymbol{k})$ by their arguments. Now, in order to clarify the relationship between constitutive operators and microgeometry, the kernel functions $\rho(\omega,\boldsymbol{k})$ and $\chi^{-1}(\omega,\boldsymbol{k})$ are needed to be determined, by introducing action-response procedures coarse-graining the dissipative fluid dynamics of the pore scale.

2.3. Procedures to compute effective density and bulk modulus

In the 1D case of macroscopic propagation along a symmetry axis, for instance x-axis with the unit vector $\hat{\boldsymbol{x}}$, we will have $\boldsymbol{D} = D\hat{\boldsymbol{x}}$ and $\boldsymbol{V} = V\hat{\boldsymbol{x}}$, $\boldsymbol{r} = x\hat{\boldsymbol{x}}$, and $\boldsymbol{k} = k\hat{\boldsymbol{x}}$ in the above equations (3–7). To determine the Fourier functions $\rho(\omega, k)$ and $\chi^{-1}(\omega, k)$ for the 1D acoustic propagation in a medium with porosity ϕ, we solve two independent action-response problems (see section 4 in [1]). For computing the effective density we consider the macroscopic response of the fluid subject to a single-component (ω, k) Fourier bulk force. The effective bulk modulus is related to the response of the fluid subject to a single-component Fourier rate of heat supply.

Two sets of equations to be solved: the two systems of equations to be solved are written as
In the fluid region $\mathcal{V}_f$:

$$\frac{\partial b}{\partial t} + \nabla \cdot \boldsymbol{v} = 0 \tag{8a}$$

$$\rho_0 \frac{\partial \boldsymbol{v}}{\partial t} = -\nabla p + \eta \nabla^2 \boldsymbol{v} + \left(\zeta + \frac{1}{3}\eta\right) \nabla (\nabla \cdot \boldsymbol{v}) + \underbrace{\boldsymbol{F} \mathrm{e}^{-\mathrm{i}\omega t + \mathrm{i}kx}}_{\text{added for determination of density}} \tag{8b}$$

$$\rho_0 c_p \frac{\partial \tau}{\partial t} = \beta_0 T_0 \frac{\partial p}{\partial t} + \kappa \nabla^2 \tau + \underbrace{\dot{Q}\, \mathrm{e}^{-\mathrm{i}\omega t + \mathrm{i}kx}}_{\text{added for determination of bulk modulus}} \tag{8c}$$

$$\gamma \chi_0 p = b + \beta_0 \tau \tag{8d}$$

On the fluid/solid interface $\partial\mathcal{V}$:

$$\boldsymbol{v} = 0, \qquad \tau = 0 \tag{9}$$

For convenience, the excitation amplitudes are written as: $\dot{Q}\, \mathrm{e}^{-\mathrm{i}\omega t + \mathrm{i}kx} = \beta_0 T_0 (\partial/\partial t) \left(\mathcal{P} \mathrm{e}^{-\mathrm{i}\omega t + \mathrm{i}kx}\right)$, and $\boldsymbol{F} \mathrm{e}^{-\mathrm{i}\omega t + \mathrm{i}kx} = -\nabla \left(\mathcal{P} \mathrm{e}^{-\mathrm{i}\omega t + \mathrm{i}kx}\right)$. Here, it is important to note that the excitation variables ω and k are set as independent variables. The solutions to the above systems for the fields p, b, τ, and components of $\boldsymbol{v}$ take the form $p(t, \boldsymbol{r}) = p(\omega, k, \boldsymbol{r}) \mathrm{e}^{-\mathrm{i}\omega t + \mathrm{i}kx}$, and so on. Recall that the theory is formulated for a geometry that is stationary random, and the averaging operator $\langle\,\rangle$ refers to the ensemble averaging. Thus, here, the amplitude fields $\boldsymbol{v}(\omega, k, \boldsymbol{r})$, $p(\omega, k, \boldsymbol{r})$, $b(\omega, k, \boldsymbol{r})$, and $\tau(\omega, k, \boldsymbol{r})$, are stationary random functions of $\boldsymbol{r}$. Passing to the case of periodic geometry, we can limit ourselves to considering one periodic sample. The fields become periodic functions over a cell, and $\langle\,\rangle$ is interpreted as a volume average over a cell.

Effective density and bulk modulus: Once the two systems of equations are solved independently, using the right hand Maxwellian macroscopic equations in (3) and (4), we arrive at the following expressions for the nonlocal effective density and bulk modulus

$$\rho(\omega, k) = \frac{k\,(\mathcal{P} + P(\omega, k))}{\omega \langle v(\omega, k, \boldsymbol{r}) \rangle} \tag{10a}$$

$$\chi^{-1}(\omega, k) = \frac{P(\omega, k) + \mathcal{P}}{\langle b(\omega, k, \boldsymbol{r}) \rangle + \phi \gamma \chi_0 \mathcal{P}} \tag{10b}$$

where $P\langle \boldsymbol{v} \rangle = \langle p \boldsymbol{v} \rangle$, which has been inspired by (7).

Wavenumbers: Contrary to the case of local theory, here, since we fully take into account spatial dispersion, several normal mode solutions might exist, with fields varying as $\mathrm{e}^{-\mathrm{i}\omega t + \mathrm{i}kx}$. Each solution should satisfy the following dispersion equation

$$\rho(\omega, k) \chi(\omega, k) \omega^2 = k^2 \tag{11}$$

which is easily derived from the Maxwellian macroscopic equations. With each frequency ω, several complex wavenumbers $k_l(\omega)$, $\Im(k_l) > 0$, $l = 1, 2, \ldots$, may be associated.

In what follows, with the aim of obtaining the nonlocal effective density, effective bulk modulus, and wavenumber of the least attenuated mode, we will apply this theoretical framework in analytical simplified manner, to a 2D array of Helmholtz resonators, illustrated in Fig. 1 right. Sound propagation through this material exhibits resonance phenomena resulting in metamaterial behavior.

3. Nonlocal modeling for 2D structure

We proceed to determine the functions $\rho(\omega, k)$ and $\chi^{-1}(\omega, k)$ sufficiently precise to give an appropriate modeling of the least attenuated mode, which results then in purely frequency dependent functions $\rho(\omega)$ and $\chi^{-1}(\omega)$. For this purpose, we do not need to consider in full detail the microscopic fields $\boldsymbol{v}$ and p. In the waveguide t and cavity c, instead of the microscopic fields, we can use the mean values $V_{t(c)} = \langle \boldsymbol{v} \rangle_S \cdot \hat{\boldsymbol{x}}$ and $P_{t(c)} = \langle p \rangle_S$, where $\langle\,\rangle_S$ denotes the average at a given x over the waveguide or the cavity width; and in the neck n, we can use the mean values $V_n = \langle \boldsymbol{v} \rangle_S \cdot \hat{\boldsymbol{y}}$ and $P_n = \langle p \rangle_S$,

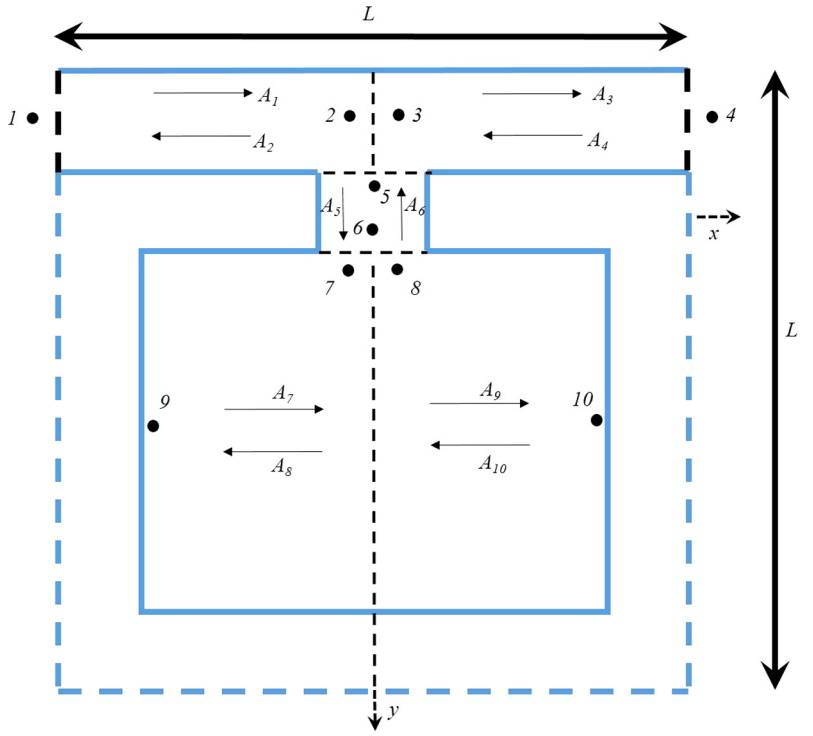

Fig. 2. (Color online.) Illustration of slit portions and plane waves propagating in different parts of the resonator. Different positions are indicated by m, and different amplitudes by A_m, $m = 1, \ldots, 10$.

where $\langle\,\rangle_S$ denotes the average at a given y over the neck width, and $\hat{\boldsymbol{y}}$ is the unit vector in the y direction. At the same time, we make some simplifications consistent with describing the propagation of these averaged quantities in terms of the Zwikker and Kosten densities $\rho(\omega)$ and bulk moduli $\chi^{-1}(\omega)$, in the different slit portions. These depend only on the slit half-widths, which we shall denote by s_t, s_n, and s_c, in the tube, neck, and cavity, respectively. The different slit-like tube portions are illustrated in Fig. 2. The main tube t is divided in two Zwikker and Kosten ducts, a left duct, and a right duct, oriented in the x direction. The same separation is made for the cavity c, whereas the neck n is not divided but viewed as one Zwikker and Kosten duct oriented in y direction.

3.1. Determination of nonlocal effective density

Considering the periodic cell of Fig. 1 right, and the corresponding cell average operation $\langle\,\rangle$, we look for the response of the fluid when a harmonic driving force $f(t,x) = f\mathrm{e}^{-\mathrm{i}\omega t+\mathrm{i}kx}$ in the direction of $\hat{\boldsymbol{x}}$ is applied. If we can determine the microscopic response velocity and pressure fields $\boldsymbol{v}$, p, then we will have the function $\rho(\omega,k)$ through the relation (see Eq. (10a))

$$\rho(\omega,k) = \frac{f - \mathrm{i}k\mathtt{P}(\omega,\mathrm{k})}{-\mathrm{i}\omega\langle v(\omega,k,\boldsymbol{r})\rangle} \tag{12}$$

with $\mathtt{P}(\omega,k) = \langle pv\rangle / \langle v\rangle$, where the v is the x-component of the microscopic velocity $\boldsymbol{v}$.

In [26, Appendix], the Zwikker and Kosten local theory is expressed for tubes of circular cross-section. For 2D slits, exactly the same general principles of modeling may be used; only some details of the calculations are changed. In particular, the Bessel functions J_0 and J_1 are replaced by cosh and sinh functions. Zwikker and Kosten's effective densities $\rho_\alpha(\omega)$ and bulk moduli $\chi_\alpha^{-1}(\omega)$ in the guide, neck and cavity, will be [27]

$$\rho_\alpha(\omega) = \rho_0\left[1 - \frac{\tanh\left(\sqrt{-\mathrm{i}\omega\rho_0 s_\alpha^2/\eta}\right)}{\sqrt{-\mathrm{i}\omega\rho_0 s_\alpha^2/\eta}}\right]^{-1},\quad \chi_\alpha^{-1}(\omega) = \gamma P_0\left[1 + (\gamma-1)\frac{\tanh\left(\sqrt{-\mathrm{i}\omega\rho_0 c_p s_\alpha^2/\kappa}\right)}{\sqrt{-\mathrm{i}\omega\rho_0 c_p s_\alpha^2/\kappa}}\right]^{-1} \tag{13}$$

for $\alpha = t, n, c$, where the indexes t, n, and c are related to the tube, neck, and cavity, respectively; P_0 the fluid pressure at rest. The corresponding wavenumbers $k_\alpha(\omega)$ and characteristic admittances $Y_\alpha(\omega)$ are expressed as $k_\alpha = \omega/c_\alpha$, and $Y_\alpha(\omega) = 2s_\alpha/(\rho_\alpha c_\alpha)$, for $\alpha = t, n, c$, where $c_\alpha = 1/\sqrt{\rho_\alpha \chi_\alpha}$, is the corresponding Zwikker and Kosten's phase velocity. Notice

that we include the slit width $2s_\alpha$ (resp. Σ, σ, and $L-\Sigma-2l$ in the resonator, see Fig. 1 left) in the definition of the characteristic admittance, because it simplifies the subsequent writing of continuity conditions.

We start writing the Zwikker and Kosten's equations in the different parts of the periodic cell. For the tube and the cavity, i.e., $\alpha = t, c$, we have

$$-\mathrm{i}\omega\frac{\rho_\alpha(\omega)}{S_\alpha}V_\alpha = -\frac{\partial P_\alpha}{\partial x} + f\mathrm{e}^{\mathrm{i}kx} \tag{14a}$$

$$\mathrm{i}\omega S_\alpha \chi_\alpha(\omega) P_\alpha = \frac{\partial V_\alpha}{\partial x} \tag{14b}$$

where $V_\alpha = V_x S_\alpha$ is the flow rate field across the cross section S_α, with V_x the x-component of the velocity in the sense of Zwikker and Kosten (averaged over the section), and P_α is the Zwikker and Kosten's pressure. In the neck, the external excitation having no y-component, we have

$$\mathrm{i}\omega\frac{\rho_n(\omega)}{\sigma}V_n = \frac{\partial P_n}{\partial y} \tag{15a}$$

$$\mathrm{i}\omega\sigma\chi_n(\omega)P_n = \frac{\partial V_n}{\partial y} \tag{15b}$$

where $V_n = V_y\sigma$ is the flow rate, with V_y the y-component of the velocity, and P_n is the Zwikker and Kosten's pressure in the neck.

The general solution of the non-homogeneous equations in the tube and the cavity, (P_α, V_α), $\alpha = t, c$, is written as the sum of the general solution $(P_{\alpha,h}, V_{\alpha,h})$ of the homogeneous equations and a particular solution $(P_{\alpha,p}, V_{\alpha,p})$ of the non-homogeneous equations. A general solution of the homogeneous equations (14) is written as

$$\begin{pmatrix} P_{\alpha,h} \\ V_{\alpha,h} \end{pmatrix} = \begin{pmatrix} 1 \\ Y_\alpha \end{pmatrix} A^+\mathrm{e}^{\mathrm{i}k_\alpha x} + \begin{pmatrix} 1 \\ -Y_\alpha \end{pmatrix} A^-\mathrm{e}^{-\mathrm{i}k_\alpha x} \tag{16}$$

where A^+ and A^- are the amplitudes of the plane waves in direction of the positive x-axis and negative x-axis, respectively. The following particular solution can be considered

$$\begin{pmatrix} P_{\alpha,p} \\ V_{\alpha,p} \end{pmatrix} = \begin{pmatrix} B_\alpha \\ C_\alpha \end{pmatrix} f\mathrm{e}^{\mathrm{i}kx} \tag{17}$$

where B_α and C_α represent four constants (for each ω) to be determined. Substituting (17) in (14) gives the four constants $B_t = \mathrm{i}k/(\omega^2\rho_t\chi_t - k^2)$, $C_t = \mathrm{i}\omega\chi_t\Sigma/(\omega^2\rho_t\chi_t - k^2)$, $B_c = \mathrm{i}k/(\omega^2\rho_c\chi_c - k^2)$, and $C_c = \mathrm{i}\omega\chi_c(L-\Sigma-2l)/(\omega^2\rho_c\chi_c - k^2)$. The particular solution is the same in the left and right portions of the tube and the cavity. On the contrary and because of the presence of the neck, the general solution will have different amplitude constants in the left and right portions. Thus, the general solution of Eqs. (14) can be written as:

$$\begin{pmatrix} P_t \\ V_t \end{pmatrix} = \begin{pmatrix} 1 \\ Y_t \end{pmatrix} A_{1,3} f\mathrm{e}^{\mathrm{i}k_t x} + \begin{pmatrix} 1 \\ -Y_t \end{pmatrix} A_{2,4} f\mathrm{e}^{-\mathrm{i}k_t x} + \begin{pmatrix} B_t \\ C_t \end{pmatrix} f\mathrm{e}^{\mathrm{i}kx} \tag{18a}$$

$$\begin{pmatrix} P_c \\ V_c \end{pmatrix} = \begin{pmatrix} 1 \\ Y_c \end{pmatrix} A_{7,9} f\mathrm{e}^{\mathrm{i}k_c x} + \begin{pmatrix} 1 \\ -Y_c \end{pmatrix} A_{8,10} f\mathrm{e}^{-\mathrm{i}k_c x} + \begin{pmatrix} B_c \\ C_c \end{pmatrix} f\mathrm{e}^{\mathrm{i}kx} \tag{18b}$$

where (18a) with amplitudes A_1 and A_2 corresponds to the left-hand part of the tube, and with amplitudes A_3 and A_4 to the right-hand part (Fig. 2); similarly for (18b): A_7 and A_8 for the left part of the cavity, and A_9 and A_{10} for the right part (Fig. 2). These eight amplitudes are to be determined. The general solution of Eqs. (15), (P_n, V_n) has the form

$$\begin{pmatrix} P_n \\ V_n \end{pmatrix} = \begin{pmatrix} 1 \\ Y_n \end{pmatrix} A_5 f\mathrm{e}^{\mathrm{i}k_n y} + \begin{pmatrix} 1 \\ -Y_n \end{pmatrix} A_6 f\mathrm{e}^{-\mathrm{i}k_n y} \tag{19}$$

where A_5 and A_6 are the neck amplitude-relating constants to be determined (Fig. 2).

Indeed, in the framework of our simple plane-wave modeling, there are 10 relations concerning the flow rate and pressure, which are assumed to be verified. These continuity relations involve the values of the fields at different locations indicated by numbers $m = 1, \ldots, 10$, in Fig. 2. We now proceed to write them.

The Bloch condition results in $P_t^{(4)} = \mathrm{e}^{\mathrm{i}kL}P_t^{(1)}$ and $V_t^{(4)} = \mathrm{e}^{\mathrm{i}kL}V_t^{(1)}$. Then $A_3\mathrm{e}^{\mathrm{i}k_tL/2} + A_4\mathrm{e}^{-\mathrm{i}k_tL/2} = \mathrm{e}^{\mathrm{i}kL}(A_1\mathrm{e}^{-\mathrm{i}k_tL/2} + A_2\mathrm{e}^{\mathrm{i}k_tL/2})$ and $A_3\mathrm{e}^{\mathrm{i}k_tL/2} - A_4\mathrm{e}^{-\mathrm{i}k_tL/2} = \mathrm{e}^{\mathrm{i}kL}(A_1\mathrm{e}^{-\mathrm{i}k_tL/2} - A_2\mathrm{e}^{\mathrm{i}k_tL/2})$. We assume the continuity of the pressure at the junction (2)–(3), $P_t^{(3)} = P_t^{(2)}$, then $A_3 + A_4 = A_1 + A_2$. We assume the continuity of the pressure at the junction (5)–(2), $P_n^{(5)} = P_t^{(2)}$, then $A_5\mathrm{e}^{-\mathrm{i}k_nl/2} + A_6\mathrm{e}^{\mathrm{i}k_nl/2} = A_1 + A_2 + B_t$. The flow rate at the junction (2)–(3)–(5) is assumed to verify $V_t^{(2)} - V_t^{(3)} = V_n^{(5)}$, which yields $Y_t\left(A_1 - A_2 - A_3 + A^4\right) = Y_n\left(A_5\mathrm{e}^{-\mathrm{i}k_nl/2} - A_6\mathrm{e}^{\mathrm{i}k_nl/2}\right)$. The continuity of the pressure at the junction (6)–(7), $P_n^{(6)} = P_c^{(7)}$ results in $A_5\mathrm{e}^{\mathrm{i}k_nl/2} + A_6\mathrm{e}^{-\mathrm{i}k_nl/2} = A_7 + A_8 + B_c$. The flow rate at the junction (6)–(7)–(8) is assumed to

verify $V_n^{(6)} + V_c^{(7)} = V_c^{(8)}$, therefore $Y_n\left(A_5 e^{ik_n l/2} - A_6 e^{-ik_n l/2}\right) + Y_c(A_7 - A_8) = Y_c(A_9 - A_{10})$. The pressure is continuous at (7)–(8), $P_c^{(7)} = P_c^{(8)}$, then $A_7 + A_8 = A_9 + A_{10}$. The flow rate vanishes at the interface solid–fluid, $V_c^{(9)} = 0$; we have $Y_c\left[A_7 e^{-ik_c(L-l)/2} - A_8 e^{ik_c(L-l)/2}\right] = -C_c e^{-ik(L-l)/2}$. The flow rate vanishes at the interface solid–fluid, $V_c^{(10)} = 0$, thus $Y_c\left[A_9 e^{ik_c(L-l)/2} - A_{10} e^{-ik_c(L-l)/2}\right] = -C_c e^{ik(L-l)/2}$.

As such, we have 10 equations for 10 unknown amplitudes $A_1, \ldots, A_{10}$. Once these are determined, we will have all the Zwikker and Kosten's fields through Eqs. (18) and (19). At this point, we can easily obtain the cell averages $\langle v\rangle$ and $\langle pv\rangle$. Let us start with $\langle v\rangle$ regarding the fact that the Zwikker and Kosten's flow rate has no component along the y-axis

$$\langle v\rangle = \frac{1}{L^2}\left(\int_{-L/2}^{0} V_t\,dx + \int_{0}^{L/2} V_t\,dx + \int_{-(L-l)/2}^{0} V_c\,dx + \int_{0}^{(L-l)/2} V_c\,dx\right) \tag{20}$$

Similarly, we can compute $\langle pv\rangle$ through the following relation:

$$\langle pv\rangle = \frac{1}{L^2}\left(\int_{-L/2}^{0} P_t V_t\,dx + \int_{0}^{L/2} P_t V_t\,dx + \int_{-(L-l)/2}^{0} P_c V_c\,dx + \int_{0}^{(L-l)/2} P_c V_c\,dx\right) \tag{21}$$

Now, we can obtain explicitly the effective density function $\rho(\omega, k)$ through Eq. (12). In the next section, the effective bulk modulus is computed in a similar way, but with a different excitation term, and with exactly the same conditions on the flow rate and pressure fields at different junctions.

3.2. Determination of nonlocal effective bulk modulus

Considering the periodic cell (Fig. 2), when a harmonic heating $\dot{Q}(t,x) = \dot{Q}_0 e^{-i\omega t + ikx} = -i\omega\beta_0 T_0 \mathcal{P} e^{-i\omega t + ikx}$ is applied in the medium, we write the Zwikker and Kosten's equations, in each part of the resonator: tube, neck, and cavity. The aim is to obtain the function $\chi^{-1}(\omega, k)$ as it is indicated in Eq. (10b). In the main tube and the cavity, for $\alpha = t, c$, we write:

$$-i\omega\frac{\rho_\alpha(\omega)}{S_\alpha}V_\alpha = -\frac{\partial P_\alpha}{\partial x} \tag{22a}$$

$$i\omega S_\alpha \chi_\alpha(\omega) P_\alpha + i\omega S_\alpha\left(\chi_\alpha(\omega) - \gamma\chi_0\right)\mathcal{P} = \frac{\partial V_\alpha}{\partial x} \tag{22b}$$

The second term in the second equation might not seem to be obvious, but follows the very procedure of obtaining (10b). In the neck, the equations are written as

$$i\omega\frac{\rho_n(\omega)}{\sigma}V_n = \frac{\partial P_n}{\partial y} \tag{23a}$$

$$i\omega\sigma\,\chi_n(\omega) P_n + i\omega\sigma\left(\chi_n(\omega) - \gamma\chi_0\right)\mathcal{P}\left\langle e^{ikx}\right\rangle_\sigma = \frac{\partial V_n}{\partial y} \tag{23b}$$

where the term $\mathcal{P}\langle e^{ikx}\rangle_\sigma$ comes from the averaging of $\dot{Q}$ over the neck cross section. Here also, the second equation might not appear obvious, but follows the procedure of the determination of (10b) in nonlocal theory [1].

As in Section 3.1, the general solution of the non-homogeneous equations (22) in the right or left part of the tube and the cavity, is written as the sum of the general solution $(P_{\alpha,h}, V_{\alpha,h})$ of the homogeneous equations and a particular solution $(P_{\alpha,p}, V_{\alpha,p})$ of the non-homogeneous equations. A general solution of the homogeneous equations (22) is written as Eq. (16). The following particular solution can be considered

$$\begin{pmatrix} P_{\alpha,p} \\ V_{\alpha,p}\end{pmatrix} = \begin{pmatrix} B_\alpha \\ C_\alpha\end{pmatrix}\mathcal{P} e^{ikx} \tag{24}$$

where B_α and C_α are four constants to be determined. Substituting (24) in (22) gives the four constants $B_t = \omega^2\rho_t(\chi_t - \gamma\chi_0)/(k^2 - \omega^2\rho_t\chi_t)$, $C_t = \omega k(\chi_t - \gamma\chi_0)\Sigma/(k^2 - \omega^2\rho_t\chi_t)$, $B_c = \omega^2\rho_c(\chi_c - \gamma\chi_0)/(k^2 - \omega^2\rho_c\chi_c)$, and $C_c = \omega k(\chi_t - \gamma\chi_0)(L - \Sigma - 2L)/(k^2 - \omega^2\rho_c\chi_c)$. Thus, the general solution of Eqs. (22) can be written as Eqs. (18), replacing f with $\mathcal{P}$. The amplitudes A_1, A_2, A_3, A_4, A_7, A_8, A_9, and A_{10} (Fig. 2) are to be determined.

As for the tube and the cavity, the general solution of the non-homogeneous equations (23) in the neck, is written as the sum of the general solution $(P_{n,h}, V_{n,h})$ of the homogeneous equations and a particular solution $(P_{n,p}, V_{n,p})$ of the non-homogeneous equations. We can find a particular solution in the following form

$$\begin{pmatrix} P_{n,p} \\ V_{n,p}\end{pmatrix} = \begin{pmatrix} B_n \\ C_n\end{pmatrix}\mathcal{P} \tag{25}$$

where B_n and C_n are two constants which will be determined by substituting (25) in (23): $B_n = (2/k\sigma)(\gamma\chi_0/\chi_n - 1) \times \sin(k\sigma/2)$, and $C_n = 0$. To obtain the above expression for B_n, the average $\langle e^{ikx}\rangle_\sigma$ can be easily calculated

$$\left\langle e^{ikx}\right\rangle_\sigma = \frac{1}{\sigma}\int_{-\sigma/2}^{\sigma/2} e^{ikx}dx = \frac{2}{k\sigma}\sin\frac{k\sigma}{2}$$

Therefore, the general solution of Eq. (23) in the neck can be written as

$$\begin{pmatrix} P_n \\ V_n \end{pmatrix} = \begin{pmatrix} 1 \\ Y_n \end{pmatrix} A_5 \mathcal{P} e^{ik_n y} + \begin{pmatrix} 1 \\ -Y_c \end{pmatrix} A_6 \mathcal{P} e^{-ik_n y + \begin{pmatrix} B_n \\ 0 \end{pmatrix}\mathcal{P}} \tag{26}$$

where A_5 and A_6 are amplitude-relating constants to be determined (Fig. 2).

As in the previous Section 3.1, in the framework of our modeling, there are 10 relations which are assumed to be verified, allowing to relate the flow rates and pressures at different indicated points in Fig. 2. These relations result in 10 equations by which we can compute the amplitudes $A_1, \ldots, A_{10}$. Consequently, all Zwikker and Kosten's fields will be found. The averages $\langle v\rangle$ and $\langle pv\rangle$ are found through rewriting the equations (20) and (21) for the actual fields. We need also the expression for $\langle b\rangle$ to obtain finally $\chi^{-1}(\omega, k)$. We have

$$\begin{aligned} -i\omega\langle b\rangle &= -\frac{1}{L^2}\int \nabla\cdot\boldsymbol{v}\,dx\,dy \\ &= -\frac{1}{L^2}\oint \boldsymbol{v}\cdot\boldsymbol{n}\,dS = -\frac{1}{L^2}\left(-V_t^{(1)} + V_t^{(4)}\right) \\ &= -\frac{\mathcal{P}}{L^2}\left[2iC_t\sin\frac{k_tL}{2} + Y_t\left(-A_1e^{-i\frac{k_tL}{2}} + A_2e^{i\frac{k_tL}{2}} + A_3e^{i\frac{k_tL}{2}} - A_4e^{-i\frac{k_tL}{2}}\right)\right] \end{aligned}$$

where $\boldsymbol{n}$ is the normal unit vector outward from the border of integration.

Now, we can obtain explicitly the effective bulk modulus function $\chi^{-1}(\omega, k)$ through Eq. (10b).

4. Bloch wave modeling

In this section, without using the principles of the nonlocal macroscopic theory but within the same plane wave modeling, we directly seek the macroscopic Bloch wavenumber k_B of the least attenuated wave propagating in the direction of positive x-axis, such that

$$\begin{pmatrix} P_t^{(4)} \\ V_t^{(4)} \end{pmatrix} = e^{ik_BL}\begin{pmatrix} P_t^{(1)} \\ V_t^{(1)} \end{pmatrix} \tag{27}$$

With the field constituted of 10 Zwikker and Kosten's slit waves, as illustrated in Fig. 2, are associated 10 complex amplitudes $A_1, \ldots, A_{10}$. As before, between these 10 amplitudes there are a set of 10 relations; where two of them express the Bloch condition (27), and 8 relations are based on the continuity equations. Here, all these relations are homogeneous relations, so that nontrivial solutions will be obtained only if the determinant of the coefficient matrix vanishes. This condition will give the Bloch wavenumber k_B.

The first step is to determine the entrance admittance of the resonator $Y_r = V_n^{(5)}/P_n^{(5)}$. The general solution of the homogeneous form of Eqs. (14) for the cavity, $\alpha = c$, without the forcing term, is written as

$$\begin{pmatrix} P_c \\ V_c \end{pmatrix} = \begin{pmatrix} 1 \\ Y_c \end{pmatrix} A_{7,9}e^{ik_cx} + \begin{pmatrix} 1 \\ -Y_c \end{pmatrix} A_{8,10}e^{-ik_cx} \tag{28}$$

where A_7 and A_8 are the amplitudes of the waves in the left part of the cavity, and A_9, A_{10} are the amplitudes of the waves in the right part. Regarding the above equation, the three conditions $P_c^{(7)} = P_c^{(8)}$, $V_c^{(9)} = 0$, and $V_c^{(10)} = 0$, result in the three following relations: $A_8 = A_7e^{-ik_c(L-l)}$, $A_9 = A_7e^{-ik_c(L-l)}$, and $A_{10} = A_7$. Using (28), there follows $P_c^{(7)} = A_7\left(1 - e^{ik_c(L-l)}\right)$, $V_c^{(7)} = Y_cA_7\left(1 + e^{ik_c(L-l)}\right)$, and $V_c^{(8)} = Y_cA_7(e^{ik_c(L-l)} - 1)$. Then, we can obtain the expressions for $P_n^{(6)}$ and $V_n^{(6)}$, through already indicated continuity conditions $P_n^{(6)} = P_c^{(7)}$, and $V_n^{(6)} + V_c^{(7)} = V_c^{(8)}$, which, subsequently, yields the impedance $Y_6 = V_n^{(6)}/P_n^{(6)}$:

$$Y_6 = -2iY_c\frac{1 - e^{-ik_c(L-l)}}{1 + e^{-ik_c(L-l)}} \tag{29}$$

Once $P_n^{(6)}$ and $V_n^{(6)}$ are known, we can obtain $P_n^{(5)}$ and $V_n^{(5)}$ through

Table 1
Fluid properties used in all computations (air).

ρ_0 (kg·m^{-3})	T_0 (K)	c_0 (m·s^{-1})	η (kg·m·s^{-1})	ζ (kg·m·s^{-1})	κ (W·m^{-1}·K^{-1})	χ_0 (Pa^{-1})	c_p (J·kg^{-1}·K^{-1})	γ
1.205	293.5	340.14	1.84×10^{-5}	0.6 η	2.57×10^{-2}	7.17×10^{-6}	997.54	1.4

$$\begin{pmatrix} P_n^{(5)} \\ V_n^{(5)} \end{pmatrix} = \begin{pmatrix} \cos k_n l & -\frac{\mathrm{i}}{Y_n}\sin k_n l \\ -iY_n \sin k_n l & \cos k_n l \end{pmatrix} \begin{pmatrix} P_n^{(6)} \\ V_n^{(6)} \end{pmatrix} \tag{30}$$

Hence, the impedance of the resonator Y_r is expressed as

$$Y_r = \frac{-iY_n \sin k_n l + Y_6 \cos k_n l}{\cos k_n l - i\dfrac{Y_6}{Y_n}\sin k_n l} \tag{31}$$

Now, we look for the macroscopic wavenumber k_B. The following relations are satisfied in the right and left part of the tube

$$\begin{pmatrix} P_t^{(1),(3)} \\ V_t^{(1),(3)} \end{pmatrix} = \begin{pmatrix} \cos \frac{k_t L}{2} & -\frac{\mathrm{i}}{Y_t}\sin \frac{k_t L}{2} \\ -\mathrm{i}Y_t \sin \frac{k_t L}{2} & \cos \frac{k_t L}{2} \end{pmatrix} \begin{pmatrix} P_t^{(2),(4)} \\ V_t^{(2),(4)} \end{pmatrix} \tag{32}$$

Making use of Eq. (27), the above equations result in

$$\begin{pmatrix} P_t^{(3)} \\ V_t^{(3)} \end{pmatrix} = \mathrm{e}^{\mathrm{i}k_\mathrm{B}L} \begin{pmatrix} \cos k_t L & -\frac{\mathrm{i}}{Y_t}\sin k_t L \\ -\mathrm{i}Y_t \sin k_t L & \cos k_t L \end{pmatrix} \begin{pmatrix} P_t^{(2)} \\ V_t^{(2)} \end{pmatrix} \tag{33}$$

In addition, as we have seen before, the three following conditions are assumed in the resonator: $P_t^{(3)} = P_t^{(2)}$, $P_n^{(5)} = P_t^{(2)}$, and $V_t^{(2)} - V_t^{(3)} = V_n^{(5)}$. We have immediately $P_t^{(3)} = P_t^{(2)} = (1/Y_r)\left(V_t^{(2)} - V_t^{(3)}\right)$. Writing the two equations resulting from (33), and eliminating $P_t^{(3)}$ and $P_t^{(2)}$ in these equations, gives

$$\begin{pmatrix} \frac{1}{Y_r} - \mathrm{e}^{\mathrm{i}k_\mathrm{B}L}\left(\frac{1}{Y_r}\cos k_t L - \frac{\mathrm{i}}{Y_t}\sin k_t L\right) & -\frac{1}{Y_r}\left(1 - \mathrm{e}^{\mathrm{i}k_\mathrm{B}L}\cos k_t L\right) \\ \mathrm{e}^{\mathrm{i}k_\mathrm{B}L}\left(\mathrm{i}\frac{Y_t}{Y_r}\sin k_t L - \cos k_t L\right) & 1 - \mathrm{e}^{\mathrm{i}k_\mathrm{B}L}\frac{\mathrm{i}Y_t}{Y_r}\sin k_t L \end{pmatrix} \begin{pmatrix} V_t^{(2)} \\ V_t^{(3)} \end{pmatrix} = \begin{pmatrix} 0 \\ 0 \end{pmatrix} \tag{34}$$

The determinant of the coefficient matrix must vanish if the above equations have non-zero solutions. This yields a second degree algebraic equation $\mathrm{e}^{2\mathrm{i}k_\mathrm{B}L} - D\mathrm{e}^{\mathrm{i}k_\mathrm{B}L} + 1 = 0$, with $D = 2\cos k_t L - \mathrm{i}(Y_r/Y_t)\sin k_t L$. The Bloch wavenumber is then immediately expressed as

$$k_\mathrm{B} = -\frac{\mathrm{i}}{L}\ln\left(\frac{D}{2} \pm \sqrt{\frac{D^2}{4} - 1}\right) \tag{35}$$

5. Results

Here, we present the results of the nonlocal modeling, Bloch wave modeling and FEM simulations for the two-dimensional metamaterial made of Helmholtz resonators. Once the simplified nonlocal and Bloch wave modeling are validated by the results of the FEM simulations which are based on the solutions of the exact equations (8), we employ the same nonlocal modeling framework to compute the macroscopic acoustic properties of the three-dimensional material. For both 2D and 3D structures, the resonators are filled with air as a viscothermal fluid. The fluid properties for all computations are indicated in Table 1. In 2D and 3D cases, the results relating to the wavenumber of the least attenuated mode and the effective bulk modulus of the material will be shown, versus a dimensionless frequency parameter. Moreover, we will present a simple method allowing to obtain the 2D geometry roughly equivalent to the 3D material, regarding the macroscopic dynamic behavior of the material in the resonance regime of the fundamental mode.

5.1. 2D structure filled with air

For the geometry considered in Fig. 1 right, to perform the computations, we have set $L = 1$ cm, $\Sigma = 0.2\,L$, and $\sigma = 0.015\,L$. The functions $\rho(\omega, k)$ and $\chi^{-1}(\omega, k)$ are first determined within the approximations of our nonlocal modeling in Section 3. Given these expressions, we know that according to nonlocal theory the possible wavenumbers in the medium will be the solutions of the dispersion relation (11). Solving the equation (11) by a Newton–Raphson scheme, we have checked that the obtained expressions for $\rho(\omega, k)$ and $\chi^{-1}(\omega, k)$ are such that a complex solution $k(\omega)$ to (11) exists, which is very close to the value $k_\mathrm{B}(\omega)$ in (35). The frequency dependent effective density $\rho(\omega, k(\omega)) = \rho(\omega)$, and effective bulk modulus $\chi^{-1}(\omega, k(\omega)) = \chi^{-1}(\omega)$, are then obtained by putting $k = k(\omega)$ in the aforementioned excitation terms (Sections 3.1 and 3.2).

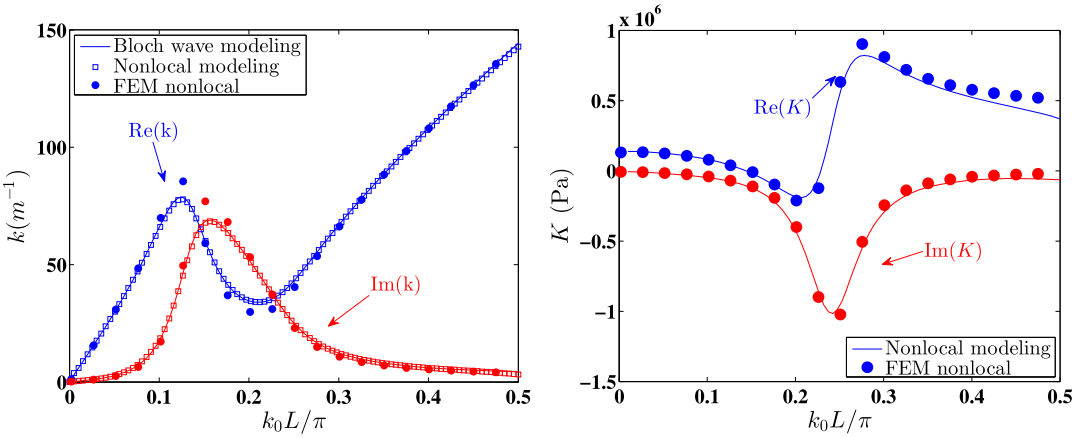

Fig. 3. (Color online.) Wavenumber (left) and bulk modulus (right) in terms of a dimensionless frequency, for the 2D structure filled with air. For the wavenumber, results by three calculations are compared: Bloch-wave modeling, nonlocal modeling, and nonlocal theory by FEM.

Solving the equation (11) by the Newton–Raphson method, we varied frequency step by step, taking as initial value for $k(\omega)$ at a given frequency, the solution value obtained at the preceding frequency. Only for the starting frequency ω_0 in the range of interest, we have chosen the value $k_B(\omega_0)$ with a 10% discrepancy.

In order to ascertain the validity of the modeling, we have also performed direct FEM simulations to solve the action-response problems, giving, subsequently, FEM evaluations of the functions $\rho(\omega,k)$ and $\chi^{-1}(\omega,k)$. Based on these functions, the computation of the wavenumber of the least attenuated wave was performed in the same way as just seen, with the only difference that (due to computation time) the initial $k(\omega)$ value at a given frequency was systematically taken to be $k_B(\omega)$ with 10% discrepancy. Finally, FEM evaluations of the frequency dependent effective density $\rho(\omega,k(\omega))=\rho(\omega)$, and effective bulk modulus $\chi^{-1}(\omega,k(\omega))=\chi^{-1}(\omega)$, were obtained by putting $k=k(\omega)$ in the aforementioned excitation terms.

The FEM computations have been performed using FreeFem++ [28], an open source tool solving partial differential equations. Adaptive meshing was employed. According to all of the calculations, the effective density remains practically constant and, therefore, does not play an important role in the macroscopic dynamics of this material.

We see in Fig. 3 left, that the real and imaginary parts of $k(\omega)$ computed by nonlocal theory via Newton's method converge exactly to the real and imaginary parts of k_B which have been computed by a simple Bloch-wave modeling without any use of nonlocal theory. The horizontal axis is the dimensionless frequency k_0L/π, where $k_0=\omega/c_0$. The results based on the FEM simulations are also in good agreement with those obtained by the Bloch wave modeling and nonlocal modeling. The frequency range has been chosen so that it covers the resonance regime. In the same frequency range, Fig. 3 right, shows the real and imaginary parts of $K(\omega)=\phi\chi^{-1}(\omega)$, representing the effective bulk modulus, computed by nonlocal FEM simulations and nonlocal modeling. Here also, we see excellent agreement between the two calculations. We notice the metamaterial behavior demonstrated in the real part of effective bulk modulus which becomes negative in a frequency range within the resonance regime. It is clear that the results by FEM computations based on the exact microscopic equations, can be considered more precise compared with our two modeling results in which we have applied simplifying approximations. As such, the good agreement between FEM results and others, validate the modeling framework. The discrepancies between the results based on the models and FEM simulations can be due in particular, to the fact that the model describes the admittance of the resonator Y_r, without considering the length correction of the neck; what might generate errors in the calculation of the wavenumber.

We observe here the same kind of behavior for the wavenumber and bulk modulus as it has been demonstrated experimentally in [23] (see Figs. 1 and 2 in that reference) for the case of the 3D material embedded in water. We have observed that removing the thermal effects by decreasing the coefficient of thermal conductivity κ to a value close to zero, would have a negligible effect on the wavenumber and the effective bulk modulus. That is the case also for the second viscosity ζ, associated with losses in the compressional/dilatational motions in the bulk fluid. On the contrary, the material dynamics in terms of the macroscopic wavenumber and bulk modulus is quite sensitive to the values of the shear viscosity η. In a frequency range, for instance, between $k_0L/\pi=0.1$ and 0.4, a maximum and minimum appear for the real part of the wavenumber. By decreasing the value of the shear viscosity, the maximum becomes sharper and finally diverges as the viscosity tends to zero at the resonance frequency of the ideal fluid $\omega_H=c_0[\sigma/l(L-2l)(L-\Sigma-2l)]^{\frac{1}{2}}$, namely $k_0L/\pi=0.15$ here; the minimum flattens and a band gap is created. As a matter of fact, the important feature, here, is the resonant behavior that induces important values of the velocity in the neck, and thus also important viscous dissipation. Furthermore, at small enough η, at frequencies close but smaller than resonance frequency, the corresponding neck flow becomes predominant and the effective wavelength is drastically reduced, leading to a so-called *slow speed*. However, when the shear viscosity increases, the neck flow adjusts to a smaller value, eventually leading to the disappearance of the *slow speed*. The viscous losses also smooth out the extrema of the real and imaginary parts of the modulus in Fig. 3 right. Consequently, a wider frequency range of the negative real part of the bulk modulus is achieved by increasing the viscous losses. The

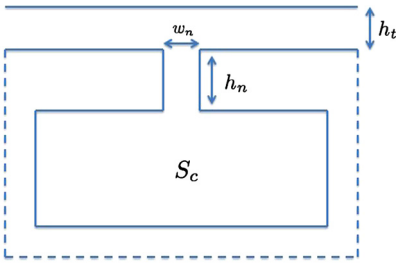

Fig. 4. (Color online.) Schematic of the 2D periodic unit of an array of Helmholtz resonator. Shown here are the geometrical parameters, which should be obtained in order to have a 2D equivalent of the 3D structure.

thermal boundary layers close to the cavity walls, where the fluid bulk modulus passes from adiabatic to isothermal value, mainly bring a small correction to the cavity spring constant (the cavity dimension is much larger than the boundary layer thickness $\delta_t = (2\kappa/\rho_0 c_p \omega)^{\frac{1}{2}}$). Therefore, their presence do not affect much the effective bulk modulus.

As explained before, the dynamics of the material will be very sensitive to the width of the neck, where a considerable part of the viscous losses take place. In our case (see values of the parameters in Fig. 1), between the frequencies $k_0 L/\pi = 0.1$ and 0.4, the ratio of the viscous boundary layer thickness $\delta_v = (2\eta/\rho_0\omega)^{\frac{1}{2}}$ to the width of the neck, insensibly changes from 0.35 to 0.39. We observed that, in general, to maintain the similar behavior of the wavenumber and modulus, this ratio should remain in the same order, regardless of changing the scale of the material or the saturating fluid. Here, well above the resonance, at $k_0 L/\pi = 0.5$, we can check that the effective wavelength in the material λ_{eff} is comparable to that in air λ_0: $\lambda_{eff}/L \sim 5$, and $\lambda_0/L = 4$. At the resonance frequency $k_0 L/\pi = 0.15$, we find that $\lambda_{eff}/L \sim 8$. Roughly, this is a reduction by a factor of two of the wavelength in air ($\lambda_0/L \sim 13.33$), and an illustration of the mentioned trend of a *slow speed* close to the resonance. Although this structure represents a subwavelength material, and therefore, can be regarded in the large wavelength limit $\lambda_{eff} \gg L$, the local theory based on the two-scale homogenization at order zero does not predict correctly the acoustics, ignoring the resonance behavior. The origin of the failure is the presence of widely different length scales, allowing for resonances.

Once the simplifying assumptions within our two modeling schemes have been validated by the precise results of the FEM simulations, we can use the same modeling framework to treat the case of 3D material.

5.2. 3D structure filled with air

Here, the resonators are placed in a periodicity $L = 1$ cm, composed of a rectangular cavity of volume $8.5 \times 5 \times 5$ mm, a cylindrical neck $l = 1$ mm long and $\sigma = 1$ mm in diameter, and a main duct portion. The neck opens in the main square air duct with a $\Sigma \times \Sigma = 0.2L \times 0.2L$ mm opening. The strategy of calculation to obtain the effective density, effective bulk modulus and the least attenuated wavenumber through nonlocal modeling and Bloch wave modeling, are the same as for 2D case in Sections 3 and 4. We can consider that the z-axis is outward from the plane of Fig. 2 which is regarded as a cross section of the 3D periodic unit. As before, Zwikker and Kosten's plane waves are propagating and attenuating in the different parts of the resonator. The only change which should be applied in the 3D calculations with respect to 2D model, is related to the Zwikker and Kosten's density and modulus which have been expressed for slits in Eq. (13). Here, we use the expressions (80) and (81) in [29] to obtain the Zwikker and Kosten's density and bulk modulus for tubes of rectangular cross section (main conduit and cavity); for the neck (tube of circular cross section) we use the expression mentioned in [26, Appendix], and also in [27,29].

Fig. 5 left, shows the real and imaginary parts of the frequency dependent wavenumber $k(\omega)$ associated with the least attenuated mode. The results based on the calculations of nonlocal modeling and Bloch wave modeling appear to be in perfect agreement. In Fig. 5 right, the real and imaginary parts of the frequency dependent bulk modulus, via $K(\omega) = \phi\chi^{-1}(\omega, k(\omega))$ are presented, according to nonlocal modeling.

Between the frequencies $k_0 L/\pi = 0.05$ and 0.3, the ratio of the viscous boundary layer to the diameter of the neck, changes from 0.15 to 0.06. Up to $k_0 L/\pi = 0.5$, the wavelength in air remains at least 4 times larger than the periodicity L. At $k_0 L/\pi = 0.5$, as in the 2D case, $\lambda_{eff}/L \sim 5$. At the resonance frequency $k_0 L/\pi = 0.07$, the effective wavelength in the material decreases to $\lambda_{eff}/L \sim 10$, which is now a reduction by a factor of 3 of the wavelength in air.

2D equivalent of the 3D structure: We have performed a simple calculation to obtain the 2D structure made of Helmholtz resonators showing roughly the same macroscopic behavior as that of a 3D structure, in particular, in terms of the wavenumber of the least attenuated mode and the effective bulk modulus. We will determine the geometrical parameters of the 2D resonator, illustrated in Fig. 4, in terms of the parameters of a 3D resonator, in a way that it exhibits resonance at the same frequency and shows approximately the same dissipative property as the 3D structure does.

In order to have roughly the same amount of both viscous and thermal losses in the main tube in 2D and 3D, it suffices to equate the hydraulic radius (see [27]). Let h_t^{2D} be the width of the tube in 2D, and h_t^{3D} the side of the square tube cross section in 3D. For the hydraulic radius be the same, we should set: $h_t^{2D} = h_t^{3D}/2$. In the same way, equating the hydraulic radius for the neck in 2D and 3D, gives the neck's width in 2D, w_n^{2D} in terms of the diameter of the circular neck cross

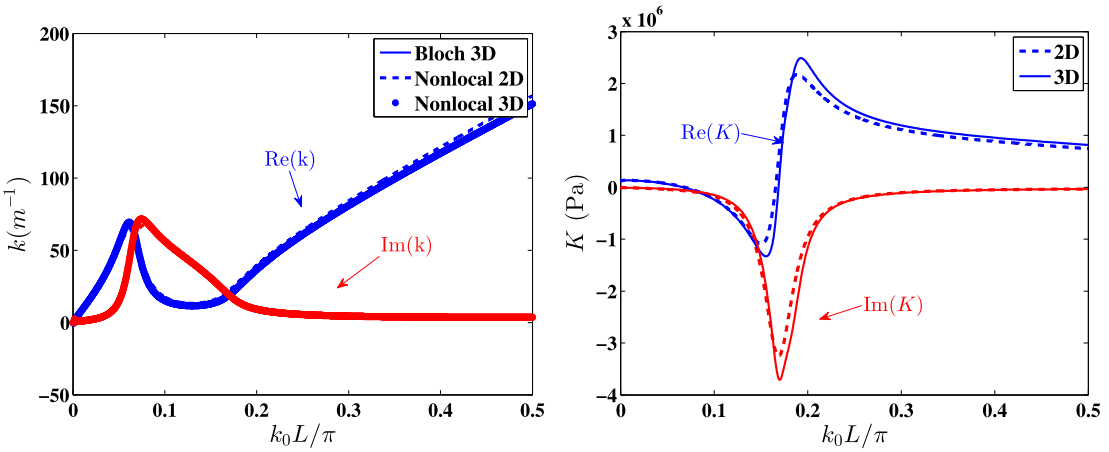

Fig. 5. (Color online.) Wavenumber (left) and bulk modulus (right) in terms of a dimensionless frequency, for the 3D structure filled with air. For the wavenumber, results by two calculations are compared: Bloch-wave modeling, nonlocal modeling.

section in 3D: $w_n^{2D} = w_n^{3D}/2$. The surface of the cavity in 2D, S_c^{2D} is determined in an intuitive manner by assuming that the ratio of the cavity volume V_c^{3D} to the tube volume V_t^{3D} in 3D is equal to the ratio of the cavity surface S_c^{2D} to the tube surface S_t^{2D} in 2D: $V_c^{3D}/V_t^{3D} = S_c^{2D}/S_t^{2D}$. We will have $S_c^{2D} = V_c^{3D}\, h_t^{2D}/(h_t^{3D})^2$. Finally, the equality of the resonance frequency in 2D, $\omega_H^{2D} = c_0(w_n^{2D}/h_n^{2D}S_c^{2D})^{\frac{1}{2}}$, and in 3D, $\omega_H^{3D} = c_0(S_n^{3D}/h_n^{3D}V_c^{3D})^{\frac{1}{2}}$, results in the expression for the neck's length in 2D: $h_n^{2D} = (V_c^{3D}\, h_n^{3D}\, w_n^{3D})/(S_n^{3D}\, S_c^{2D})$, where h_n^{3D} is the length of the neck in the 3D structure.

With the dimensions of our actual 3D structure, we find, for the geometrical parameters of the 2D version, $h_t^{2D} = 1$ mm, $w_n^{2D} = 0.24$ mm, and $h_n^{2D} = 8$ mm. We have chosen the width $w_c^{2D} = 8.5$ mm and the height $h_c^{2D} = 6.25$ mm, so that the product of them is fixed by the value of S_c^{2D}. We have also taken the same periodicity L for 2D, as in 3D. The complex wavenumber associated with the least attenuated mode, and complex effective bulk modulus of this 2D equivalent of the 3D material is depicted in Fig. 5. The complex wavenumber relating to the 2D and 3D geometries present an excellent agreement, and a very good agreement is observed regarding the real and imaginary parts of the effective bulk modulus of these two structures.

We note that, if the structure with the same geometrical parameters is embedded in water, there would be less loss as the viscous boundary layer thickness is smaller compared with that of air. To keep the same dynamic behavior with water as with air, it would be necessary to very significantly decrease the width of the neck; at this point it should be born in mind that the complicated effect of nonlinearities would certainly have to be taken into account. Furthermore the thermal effects in water are not important. The general thermodynamic identity $\gamma - 1 = \beta_0^2 T_0/\rho_0 c_p$, shows that the deviation of $\gamma \equiv c_p/c_v$ from unity, is a second order effect on the thermal expansion coefficient β_0. For a liquid, like water, β_0 is very small; what implies that γ is practically 1. In this case, adiabatic bulk modulus $\chi_{0(\text{adiab})}^{-1}$ and isothermal bulk modulus $\chi_{0(\text{isoth})}^{-1}$ are very close, since in general, $\chi_{0(\text{adiab})}^{-1} = \gamma\, \chi_{0(\text{isoth})}^{-1}$. Therefore, thermal exchanges have practically no effects.

6. Conclusion

Applying the Maxwellian nonlocal theory of sound propagation in porous media to a material with the microgeometry of the porous matrix in the form of a two or three dimensional array of Helmholtz resonators embedded in air, we have described precisely the metamaterial behavior of the dissipative medium, demonstrated by the negative real part of the effective bulk modulus in the resonance frequency regime. Using the homogenization method corresponding to the recently developed nonlocal theory, we took advantage of a plane wave modeling to obtain the effective density and bulk modulus, functions of both frequency and wavenumber. In this modeling, we made use of Zwikker and Kosten's equations governing the pressure and velocity fields' dynamics averaged over the cross-section of the different parts of the Helmholtz resonators, in order to coarse-grain them to the scale of the periodic cell containing one resonator. Once these two effective parameters have been determined, the corresponding least attenuated wavenumber of the medium could be obtained through a dispersion equation established via nonlocal theory. The frequency range has been chosen such that the geometrical-based resonance phenomena could appear.

In addition, a direct analytical modeling has been performed to obtain the least attenuated Bloch mode propagating in the medium, without using nonlocal theory. We have shown that the values of Bloch modes obtained in the direct way match exactly those computed by the nonlocal modeling. Moreover, the FEM numerical simulations allowing the computation of the effective parameters and wavenumbers without any approximation validate the results of the two modeling calculations and their simplifying assumptions. The nonlocal theory takes fully into account all viscous and thermal dissipation. However, we have observed that for this material, thermal effects are negligible, while viscous effects are quite important to describe the material's effective dynamics. We have used the same modeling framework for 3D material to

compute the effective parameters and the wavenumber of the least attenuated mode, and performed a simple calculation to find a 2D equivalent of the material, showing the same macroscopic dynamics.

Finally, the resonance-induced metamaterial behavior that we have studied here can be interpreted as a demonstration of the importance of considering the spatial dispersion in the medium. Higher order modes propagating and attenuating in this material can also be computed by the nonlocal theory. It will require, however, relaxing the plane wave simplifications made here in the modeling. This will be the subject of future research. It is significant that the nonlocal theory provides higher order modes, each of which is associated with a wavenumber and impedance or, equivalently, with a density and bulk modulus. This is a signature of the nonlocal effects which are captured by our new macroscopic approach.

Acknowledgements

We acknowledge financial support by Multidisciplinary University Research Initiative from the Office of Naval Research, Grant N00014-13-1-0631.

References

[1] D. Lafarge, N. Nemati, Nonlocal Maxwellian theory of sound propagation in fluid-saturated rigid-framed porous media, Wave Motion 50 (2013) 1016–1035.
[2] C. Zwikker, C.W. Kosten, Sound Absorbing Materials, Elsevier Publishing Company, Inc., New York, 1949, reprinted 2012 by the NAG (Nederlands Akoestisch Genootschap).
[3] D.L. Johnson, J. Koplik, R. Dashen, Theory of dynamic permeability and tortuosity in fluid-saturated porous media, J. Fluid Mech. 176 (1987) 379–402.
[4] Y. Champoux, J.F. Allard, Dynamic tortuosity and bulk modulus in air-saturated porous media, J. Appl. Phys. 70 (1991) 1975–1979.
[5] D. Lafarge, P. Lemarinier, J.F. Allard, V. Tarnow, Dynamic compressibility of air in porous structures at audible frequencies, J. Acoust. Soc. Am. 102 (1997) 1995–2006.
[6] R. Burridge, J.B. Keller, Poroelasticity equations derived from microstructure, J. Acoust. Soc. Am. 70 (1981) 1140–1146.
[7] A.N. Norris, On the viscodynamic operator in Biot's equations of poroelasticity, J. Wave-Mater. Interact. 1 (1986) 365–380.
[8] M.Y. Zhou, P. Sheng, First principles calculations of dynamic permeability in porous media, Phys. Rev. B 39 (1989) 12027–12039.
[9] D.M.J. Smeulders, R.L.G.M. Eggels, M.E.H. van Dongen, Dynamic permeability: reformulation of theory and new experimental and numerical data, J. Fluid Mech. 245 (1992) 211–227.
[10] J.L. Auriault, Dynamic behavior of a porous medium saturated by a Newtonian fluid, Int. J. Eng. Sci. 18 (1980) 775–785.
[11] J.L. Auriault, C. Boutin, C. Geindreau, Homogenization of Coupled Phenomena in Heterogenous Media, ISTE and Wiley, 2009.
[12] E. Sanchez Palencia, Nonhomogeneous Media and Vibration Theory, Lectures Notes in Physics, vol. 127, Springer, Berlin, 1980.
[13] A. Bensoussan, J.L. Lions, G.C. Papanicolaou, Asymptotic Analysis for Periodic Structure, North-Holland, Amsterdam, 1978.
[14] R.V. Craster, J. Kaplunov, A.V. Pichugin, High-frequency homogenization for periodic media, Proc. R. Soc. Lond. A 466 (2010) 2341–2362.
[15] T. Antonakakis, R.V. Craster, S. Guenneau, E.A. Skelton, An asymptotic theory for waves guided by diffraction gratings or along microstructured surfaces, Proc. R. Soc. Lond. A 470 (2013) 20130467.
[16] C. Boutin, A. Rallu, S. Hans, Large scale modulation of high frequency acoustic waves in periodic porous media, J. Acoust. Soc. Am. 132 (2012) 3622–3636.
[17] C. Boutin, Acoustics of porous media with inner resonators, J. Acoust. Soc. Am. 134 (2013) 4717–4729.
[18] M. Yang, G. Ma, Y. Wu, Z. Yang, P. Sheng, Homogenization scheme for acoustic metamaterials, Phys. Rev. B 89 (2014) 064309.
[19] Y. Wu, Y. Lai, Z.Q. Zhang, Effective medium theory for elastic metamaterials in two dimensions, Phys. Rev. B 76 (2007) 205313.
[20] C. Boutin, Sound propagation in rigid porous media: non-local macroscopic effects versus pores scale regime, Transp. Porous Media 93 (2012) 309–329.
[21] J.R. Willis, Exact effective relations for dynamics of a laminated body, Mech. Mater. 41 (2009) 385–393.
[22] L.D. Landau, E.M. Lifshitz, Electrodynamics of Continuous Media, Course of Theoretical Physics, vol. 8, Elsevier, Butterworth–Heinemann, Oxford, 2004.
[23] N. Fang, D. Xi, J. Xu, M. Ambati, W. Srituravanich, C. Sun, X. Zhang, Ultrasonic metamaterials with negative modulus, Nat. Mater. 5 (2006) 452–456.
[24] S. Zhang, L. Yin, N. Fang, Focusing ultrasound with an acoustic metamaterial network, Phys. Rev. Lett. 102 (2009) 194301.
[25] S. Zhang, C. Xia, N. Fang, Broadband acoustic cloak for ultrasound waves, Phys. Rev. Lett. 106 (2011) 24301.
[26] N. Nemati, D. Lafarge, Check on a nonlocal Maxwellian theory of sound propagation in fluid-saturated rigid-framed porous media, Wave Motion 51 (2014) 716–728.
[27] J.F. Allard, N. Atalla, Propagation of Sound in Porous Media: Modelling Sound Absorbing Materials, second edition, John Wiley & Sons, 2009.
[28] F. Hecht, New development in FreeFem++, J. Numer. Math. 20 (2012) 251–265.
[29] M.R. Stinson, The propagation of plane sound waves in narrow and wide circular tubes, and generalization to uniform tubes of arbitrary cross-sectional shape, J. Acoust. Soc. Am. 89 (1991) 550–558.